Resolution of prestack seismic migration

*Luděk Klimeš *, Department of Geophysics, Charles University Prague, Czech Republic*

Summary

Explicit approximate equations describing the physical meaning of the migrated sections are derived. The imaged combination of elastic parameters (reflectivity) depends on the selection of the polarizations of the incident and back–propagated wavefields and on the directions of propagation. The migrated section is then approximately the convolution of the unknown exact reflectivity with the resolution function depending on the aperture and on the form of the imaging time function.

Introduction

A general formulation of *prestack migration* based on imaging (mapping) incident and scattered wavefields, extrapolated into the macro–model by arbitrary numerical methods (Claerbout 1971) is considered. A *common shot* prestack migration is assumed since it is the most natural configuration from the physical point of view, although the same approach could simply be applied to other configurations. The presented theory is developed for *3-D elastic migrations* in 3-D elastic macro–models. Neither scalar acoustic wavefields nor 2-D migrations are separately investigated.

The goal of this contribution is to study the physical meaning and spatial resolution of the migrated images. Although the migrations are mostly performed in the isotropic macro–models, we shall present the equations in a general form suitable for elastic anisotropic models everywhere, where the assumption of isotropic models or perturbations enable for no considerable simplification of the theory. The equations expressed in terms of general stiffness matrix c_{ijkl} are often more concise and clear than the analogous explicit isotropic equations.

Migration

The geological structure is described in terms of the unknown material parameters

$$\varrho = \varrho(\mathbf{x}) \ , \quad c_{ijkl} = c_{ijkl}(\mathbf{x}) \quad . \tag{1}$$

The seismic macro–model of the geological structure is described in terms of the material parameters

$$\tilde{\varrho} = \tilde{\varrho}(\mathbf{x}) \ , \quad \tilde{c}_{ijkl} = \tilde{c}_{ijkl}(\mathbf{x}) \quad . \tag{2}$$

We are going to study the image of the difference

$$\Delta\varrho = \varrho - \tilde{\varrho} \ , \quad \Delta c_{ijkl} = c_{ijkl} - \tilde{c}_{ijkl} \tag{3}$$

between the geological structure and the model, obtained by means of seismic migration, for illustration see Figure 1.

In our approach, migration may be decomposed into following steps (Claerbout 1971): (a) *extrapolation* of the wavefields from the source and receiver points into the macro–model, (b) *decomposition* of the extrapolated wavefields into waves of different properties, (b) *imaging* the extrapolated and decomposed wavefields.

Extrapolation

Assume that the seismic wavefield $u_i(\mathbf{x},t)$, propagating in the geological structure of the unknown material parameters ϱ, c_{ijkl}, is recorded at the receivers covering the "receiver area" along the Earth surface with a sufficient density to allow for the back–propagation of the recorded wavefield into the model.

Let us denote by $U_i(\mathbf{x},t)$ the "scattered" wavefield back–propagated from the receiver area into the seismic macro–model. The approximate incident wavefield $\tilde{u}_i(\mathbf{x},t)$ and the back–propagated wavefield $U_i(\mathbf{x},t)$ may be calculated in the macro–model $\tilde{\varrho}(\mathbf{x})$, $\tilde{c}_{ijkl}(\mathbf{x})$ by any convenient numerical method.

Whereas seismic wavefield $u_i(\mathbf{x},t)$ in the geological structure is, approximately, subject to the elastodynamic equation

$$\varrho \frac{\partial^2 u_i}{\partial t^2} = \frac{\partial}{\partial x_j}\left[c_{ijkl}\frac{\partial u_k}{\partial x_l}\right] \quad , \tag{4}$$

seismic wavefield $\tilde{u}_i(\mathbf{x},t)$ calculated for the same source in the macro–model is subject to the elastodynamic equation

$$\tilde{\varrho} \frac{\partial^2 \tilde{u}_i}{\partial t^2} = \frac{\partial}{\partial x_j}\left[\tilde{c}_{ijkl}\frac{\partial \tilde{u}_k}{\partial x_l}\right] \quad . \tag{5}$$

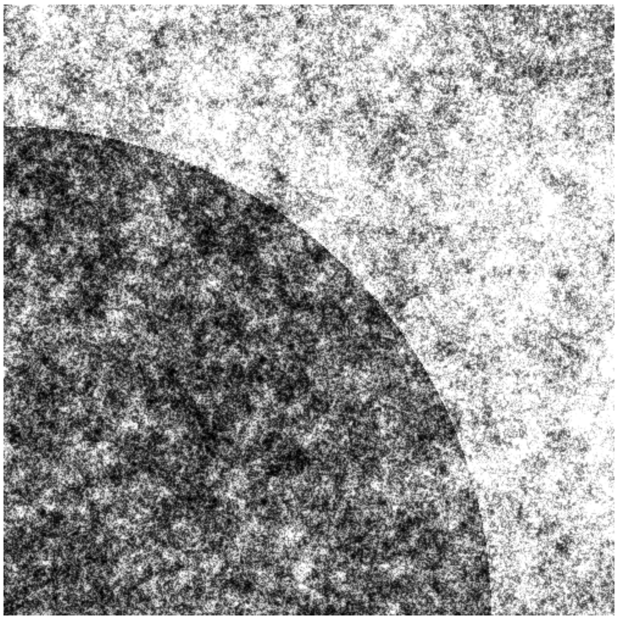

Figure 1. Structure of the target zone. Randomly generated representation of the self–affine medium is superposed with a homogeneous quarter circle in order to supplement random heterogeneities with a sharp interface. The target zone is assumed small compared with its depth below the source and receivers.

Figure 2. Common–source prestack migrated section of the structure displayed in Figure 1, simulated according to equations (11) to (13) in a homogeneous macro–model. Imaging function is the Gabor signal with the predominant wavelength of 6% the target zone dimension. Length of the symmetric receiver profile, with the source above the target zone (angle $0°$), is twice the depth of the target zone, which corresponds to aperture from $-45°$ to $45°$. Only wavenumber vectors between $-22.5°$ and $22.5°$ are thus present in the image.

Decomposition

To resolve more than a single linear combination of material perturbations $\Delta\varrho$, Δc_{ijkl}, it is desirable to attempt to decompose both the approximate incident wavefield $\tilde{u}_i(\mathbf{x},t)$ and the back–propagated wavefield $U_i(\mathbf{x},t)$ at each point $\mathbf{x}$ locally into P and S waves or, better, into P waves and two polarizations of S waves. Such a decomposition may conveniently be accomplished by a proper choice of imaging functionals, see *Imaging* below.

In addition, if the waves incident from considerably different directions can locally be distinguished in the approximate incident wavefield $\tilde{u}_i(\mathbf{x},t)$ or back–propagated wavefield $U_i(\mathbf{x},t)$, the respective wavefield should be decomposed into the parts corresponding to the different propagation directions, particularly for the purposes of the "amplitude–versus–angle" analysis.

If the decomposition into the parts corresponding to the different propagation directions is not possible, the amplitude–versus–angle analysis may be enabled by splitting the receiver area into two or more smaller receiver areas, e.g., by means of application of the aperture filter $a(\mathbf{x})$ dependent on the receiver positions $\mathbf{x}$. Such a splitting, however, deteriorates the lateral spatial resolution of the migrated sections.

If any of the above decompositions is applicable, let $\tilde{u}_i(\mathbf{x},t)$ denote hereinafter one selected part of the decomposed approximate incident wavefield and $U_i(\mathbf{x},t)$ one selected part of the back–propagated wavefield.

Imaging

Now we have, at each point $\mathbf{x}$, time functions $\tilde{u}_i(\mathbf{x},t)$ and $U_i(\mathbf{x},t)$. Assume to have "imaging functional" (mapping procedure)

$$M(\bullet,\bullet): \quad \tilde{u}_i, U_i \longrightarrow m = M(\tilde{u}_i, U_i) \quad , \tag{6}$$

mapping at each point $\mathbf{x}$ the pair of vectorial functions $\tilde{u}_i = \tilde{u}_i(t)$ and $U = U(t)$ onto the real or complex numbers, forming the migrated section $m = m(\mathbf{x})$.

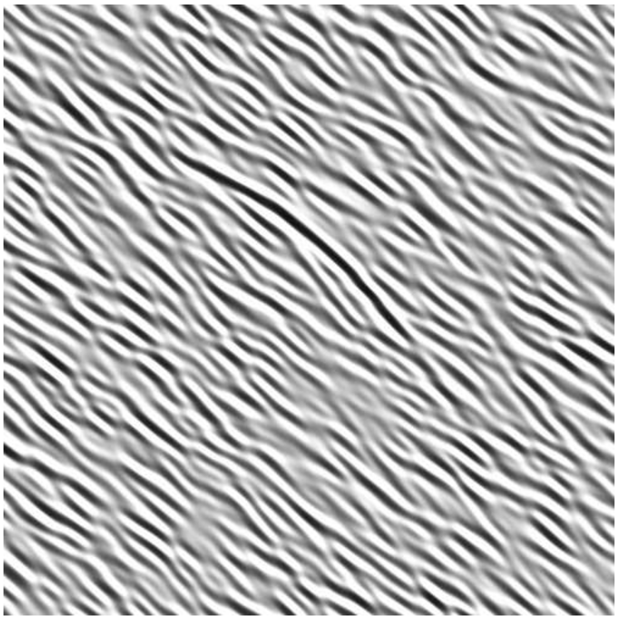

Figure 3. Common–source prestack migrated section of the structure displayed in Figure 1, simulated according to equations (11) to (13) in a homogeneous macro–model. The symmetric receiver profile from Figure 2 has been shifted to the right, locating the leftmost receiver above the target zone. The source is thus in the direction of 45° and the aperture extents from 0° to 63°. Only wavenumber vectors between 22.5° and 54° are thus present in the image.

Figure 4. Sum of the common–source prestack migrated sections of Figures 2 and 3. Let us emphasize that Figures 2, 3 and 4 are not a result of a particular migration, they show which features of the structure can be resolved by an ideal migration (no multiples, no noise, no transmission losses, perfect macro–model, exact calculation of elastic wavefields).

Let us consider a very broad class of imaging functionals of the zero–derivative form

$$M(\tilde{u}_i,U_i)=\int \mathrm{d}\omega\,\frac{\widehat{F}(\omega)\widehat{\tilde{u}}^*_j(\omega)E_{jk}\widehat{U}_k(\omega)}{\widehat{\tilde{u}}^*_m(\omega)e_{mn}\widehat{\tilde{u}}_n(\omega)}\left[\int \mathrm{d}\omega\,\widehat{F}(\omega)\right]^{-1} \quad , \tag{7}$$

or the first–derivative form

$$M(\tilde{u}_i,U_i)=\int \mathrm{d}\omega\,\frac{\widehat{F}(\omega)\widehat{\tilde{u}}^*_{i,j}(\omega)E_{ijkl}\widehat{U}_{k,l}(\omega)}{\widehat{\tilde{u}}^*_{m,r}(\omega)e_{mrns}\widehat{\tilde{u}}_{n,s}(\omega)}\left[\int \mathrm{d}\omega\,\widehat{F}(\omega)\right]^{-1} \quad , \tag{8}$$

which are the elastic analogies to the scalar imaging functionals by, e.g., Claerbout (1971), eq. (3), or Scales (1995) eq. (4). Here $\widehat{F}(\omega)$ denotes the Fourier transform of $F(t)$. The frequency range of user–defined spectral filter $\widehat{F}(\omega)$ should not exceed the frequency range of $\widehat{\tilde{u}}_i(\omega)$ or $\omega\widehat{\tilde{u}}_i(\omega)$. Many kinds of imaging functionals may be fitted by a proper choice of $\widehat{F}(\omega)$, e.g., the convolutional functionals by Claerbout (1971), eq. (4), or Stolt & Benson (1986) eq. (5.107). The spectral filter $\widehat{F}(\omega)$ directly determines the "imaging function"

$$\Phi(t)=F(t)/F(0) \quad . \tag{9}$$

The matrices $E_{jk}=E_{jk}(\mathbf{x}')$, $e_{jk}=e_{jk}(\mathbf{x}')$, $E_{ijkl}=E_{ijkl}(\mathbf{x}')$ and $e_{ijkl}=e_{ijkl}(\mathbf{x}')$ are selected in such a way to approximately decompose both the incident and back–propagated scattered wavefields into P and two S wave polarizations (Klimeš 1997).

Reflectivity function

Using the Born approximation of the back–propagated scattered wavefield, we may determine which linear combination of the material parameters is imaged by the parts $\tilde{u}_i(\mathbf{x},t)$ and $U_j(\mathbf{x},t)$ of incident and back–propagated scattered wavefields corresponding to polarizations $e_i=e_i(\mathbf{x})$ and $E_j=E_j(\mathbf{x})$, respectively (Klimeš 1997): Imaged is the is the angle–independent relative "reflectivity function"

$$R=\frac{\Delta\varrho E_m e_m+\Delta c_{mjkl}E_m P_j e_k p_l}{2\ \tilde{\varrho}} \quad , \tag{10}$$

where $p_i=p_i(\mathbf{x})$ and $P_j=P_j(\mathbf{x})$ are the corresponding slowness vectors.

Resolution of prestack seismic migration

Analysis of the migrated section

Following further the Born approximation, we can find that the migrated section has then the form of integral operator

$$m(\mathbf{x}) \approx \int \mathrm{d}x' \; S(\mathbf{x}', \mathbf{x}-\mathbf{x}') \; R(\mathbf{x}') \quad , \tag{11}$$

which has locally the character of convolution because the "resolution function" $S(\mathbf{x}', \mathbf{x}-\mathbf{x}')$ depends firstly on vector $\mathbf{x}-\mathbf{x}'$ and is just moderately varying with the location $\mathbf{x}'$. The 3-D Fourier transform of the resolution function with respect to $\mathbf{x}-\mathbf{x}'$ may be expressed in the form of

$$\widehat{S}(\mathbf{x}', \mathbf{k}) = W(\mathbf{x}', \mathbf{k}) \; \widehat{\delta}(\mathbf{k}) \quad , \tag{12}$$

where the 3-D Fourier transform $\widehat{\delta}(\mathbf{k})$ of the 3-D Dirac distribution $\delta(\mathbf{x})$ is filtered with the wavenumber filter $W(\mathbf{x}', \mathbf{k})$,

$$W\left(\mathbf{x}', [\mathbf{p}(\mathbf{x}') + \mathbf{P}(\mathbf{x}',\gamma)]\omega\right) = \frac{A(\mathbf{x}',\gamma) \; \widehat{\dot{\Phi}}(\omega)}{\tilde{v}(\mathbf{x}') \; |\mathbf{p}(\mathbf{x}') + \mathbf{P}(\mathbf{x}',\gamma)| \; \widehat{\delta}(\omega)} \quad , \tag{13}$$

specified in terms of the 1-D fourier transforms of the 1-D Dirac distribution $\delta(\Delta t)$ and the derivative $\dot{\Phi}(t)$ of the imaging function. Here $A(\mathbf{x}',\gamma)$ is the "aperture weighting function" accounting both for the aperture limitation to angular directions γ of the slowness vectors of the back–propagated wavefield and for the two–way accumulated reciprocal transmission coefficient between the target point and the receiver point.

The above filters may also be approximated by

$$m(\mathbf{x}) \approx \int \mathrm{d}x' \; s(\mathbf{x}', \mathbf{x}-\mathbf{x}') \; r(\mathbf{x}') \quad , \tag{14}$$

with

$$\widehat{s}(\mathbf{x}', \mathbf{k}) = w(\mathbf{x}', \mathbf{k}) \; \widehat{\delta}(\mathbf{k}) \tag{15}$$

and

$$w\left(\mathbf{x}', [\mathbf{p}(\mathbf{x}') + \mathbf{P}(\mathbf{x}',\gamma)]\omega\right) = \frac{A(\mathbf{x}',\gamma) \; \widehat{\Phi}(\omega)}{\widehat{\delta}(\omega)} \; \tilde{v}(\mathbf{x}') \quad , \tag{16}$$

where

$$r = \frac{\partial R}{\partial x_k} \; \frac{[p_k + P_k]}{[\tilde{v}]^2 \; |\mathbf{p} + \mathbf{P}|^3} \tag{17}$$

is the "reflection coefficient". For P-P scattering, the "reflection coefficient" (17) corresponds to the "reflection coefficient" of Stolt & Benson (1986), eq. (1.7).

The effect of convolutional filtering (11) to (13) on the structure from Figure 1 is demonstrated in Figures 2 and 3. We may assume, e.g., that the velocities are constant and that Figure 1 displays small density perturbations. Figures 2, 3 and 4 then show the images of the density which can ideally be obtained by seismic migration for a given configuration and source time function.

Conclusions

The physical meaning and spatial resolution of properly migrated sections can be estimated by means of approximate equations (10) to (17).

Acknowledgements

I am indebted to Paul Spudich who provided me with his perfect code I could modify to calculate the numerical examples presented here.
The research has been partially supported by the Grant Agency of the Czech Republic under Contract 205/95/1465, and by the consortium "Seismic Waves in Complex 3-D Structures".

References

Claerbout, J.F. (1971): Toward a unified theory of reflector mapping. Geophysics, **36**, 467–481.

Klimeš, L. (1997): Resolution of prestack seismic migration. In: Seismic Waves in Complex 3-D Structures, Report 6, Dep. Geophys., Charles Univ., Prague.

Scales, J.A. (1995): Theory of Seismic Imaging. (Lecture Notes in Earth Sciences, Vol. 55), Springer, Berlin–Heidelberg.

Stolt, R.H. & Benson, A.K. (1986): Seismic Migration. Theory and Practice. (Handbook of Geophysical Exploration, Section I: Seismic Exploration, Vol. 5), Geophysical Press, London–Amsterdam.